

# SCIENTIFIC REPORTS

OPEN

## Search for efficient inhibitors of myotoxic activity induced by ophidian phospholipase A<sub>2</sub>-like proteins using functional, structural and bioinformatics approaches

Guilherme H. M. Salvador<sup>1</sup>, Fábio Florença Cardoso<sup>1</sup>, Antoniel A. Gomes<sup>1</sup>,  
Walter L. G. Cavalcante<sup>1,2</sup>, Márcia Gallacci<sup>3</sup> & Marcos R. M. Fontes<sup>1</sup> 

Ophidian accidents are considered an important neglected tropical disease by the World Health Organization. Particularly in Latin America, *Bothrops* snakes are responsible for the majority of the snakebite envenomings that are not efficiently treated by conventional serum therapy. Thus, the search for simple and efficient inhibitors to complement this therapy is a promising research area, and a combination of functional and structural assays have been used to test candidate ligands against specific ophidian venom compounds. Herein, we tested a commercial drug (acetylsalicylic acid, ASA) and a plant compound with antiophidian properties (rosmarinic acid, RA) using myographic, crystallographic and bioinformatics experiments with a phospholipase A<sub>2</sub>-like toxin, MjTX-II. MjTX-II/RA and MjTX-II/ASA crystal structures were solved at high resolution and revealed the presence of ligands bound to different regions of the toxin. However, *in vitro* myographic assays showed that only RA is able to prevent the myotoxic effects of MjTX-II. In agreement with functional results, molecular dynamics simulations showed that the RA molecule remains tightly bound to the toxin throughout the calculations, whereas ASA molecules tend to dissociate. This approach aids the design of effective inhibitors of PLA<sub>2</sub>-like toxins and, eventually, may complement serum therapy.

Snakebite accidents caused by *Bothrops* snakes can induce severe local myonecrosis in victims, which may lead to permanent sequelae, such as drastic tissue loss, amputation and disability<sup>1–4</sup>. Serum therapy is the most used treatment for this pathology; however, the difficulty of neutralizing the local effect is a challenge, since the rapid action of toxins present in *Bothrops* venom reduces the serum efficiency<sup>1,5,6</sup>.

One class of proteins present in bothropic venom is the phospholipases A<sub>2</sub> (PLA<sub>2</sub>s), which can be divided in catalytic PLA<sub>2</sub>s and myotoxic PLA<sub>2</sub>-like proteins<sup>7–9</sup>. Several sites responsible for myotoxic activity caused by myotoxic PLA<sub>2</sub>-like proteins (including Lys49-PLA<sub>2</sub>s) were previously described and led to the current proposed myotoxic mechanism<sup>6,10–13</sup>. A step-by-step myotoxic mechanism for PLA<sub>2</sub>-like proteins was presented initially in 2014 and complemented in 2017; the mechanism consists of several steps, including: *i*) hydrophobic molecule binding at the hydrophobic channel; *ii*) protein activation - including protein reorientation and stabilization with exposure of its active sites to the solvent; *iii*) protein-membrane interaction at the membrane-docking site (MDoS); *iv*) membrane destabilization by residues at the membrane-disrupting site (MDiS); and *v*) cell death<sup>14,15</sup>.

Interestingly, myotoxin-II (MjTX-II) isolated from *Bothrops moojeni* venom presents some structural differences compared to other PLA<sub>2</sub>-like proteins from the *Bothrops* genus<sup>16,17</sup>. The changes in its amino acid sequence, including mutations in conserved residues (Leu32Gly and His121Tyr) and the insertion of an Asn residue at position 120, are reflected in structural changes in the hydrophobic channel and its interactions with long-chain molecules<sup>16–18</sup>. Furthermore, fatty acids binding to MjTX-II are not necessary for the alignment of its MDoS and

<sup>1</sup>Depto. de Física e Biofísica, Instituto de Biociências, UNESP – Universidade Estadual Paulista, Botucatu, SP, Brazil. <sup>2</sup>Depto. de Farmacologia, UFMG - Universidade Federal de Minas Gerais, Belo Horizonte, MG, Brazil. <sup>3</sup>Depto. de Farmacologia, Instituto de Biociências, UNESP – Universidade Estadual Paulista, Botucatu, SP, Brazil. Correspondence and requests for materials should be addressed to M.R.M.F. (email: [marcos.fontes@unesp.br](mailto:marcos.fontes@unesp.br))

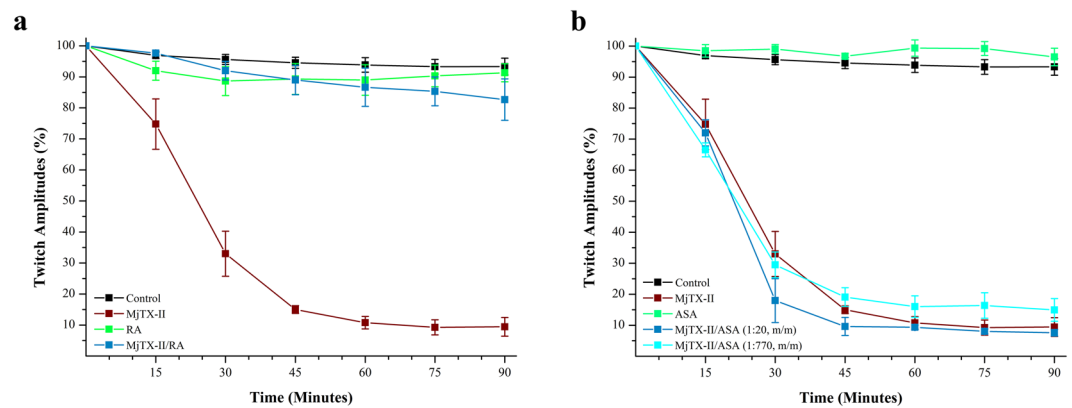


**Figure 1.** Effects of the MjTX-II and the product of its pre-incubation with (a) rosmarinic acid (RA) and (b) acetylsalicylic acid (ASA) on indirectly evoked twitches in isolated mice phrenic diaphragm preparations. The ordinate indicates the percentage of twitches relative to its initial amplitude. The abscissa indicates the time (minutes) after addition of MjTX-II, (a) rosmarinic acid or (b) acetylsalicylic acid alone and the mixture of MjTX-II plus (a) rosmarinic acid (1:10, m/m) or (b) acetylsalicylic acid (1:20, m/m and 1:770, m/m) to the organ bath. The data are grouped as means  $\pm$  SEM ( $P < 0.05$ ) and all groups have  $N = 3$ . \*Indicates the point from which there was a significant difference compared with control.

MDiS regions<sup>18</sup>; consequently, this difference is important compared to other PLA<sub>2</sub>-like toxins, since MjTX-II activation would be facilitated.

Snakebite envenomation is considered a neglected tropical disease by the World Health Organization. It leads to approximately one 100,000 deaths per year and around three times as many amputations and other permanent disabilities due to poor access to a health system and the inefficiency or lack of specific antivenoms. Thus, the search for simple and efficient inhibitors to complement serum therapy is a promising research area. In the last decade, a combination of functional, biochemical, biophysical, structural and bioinformatics tools have been used to test ligands that may be candidates to specifically inhibit ophidian venom compounds<sup>17,19–25</sup>.

Medicinal plants, which are used in folk medicine, are a source of biological active compounds, including inhibitor candidates for the snake envenoming<sup>26–30</sup>. Plants from *Boraginaceae* and *Laminaceae* families have several important biological properties, including its ability to neutralize the inflammatory, myotoxic and hemorrhagic activities of crude snake venoms and/or their isolated toxins<sup>21,31</sup>. Rosmarinic acid (RA) is a polyphenolic compound found in those plants<sup>21,32</sup>, and more recently, several studies have demonstrated the efficiency of this molecule against the myotoxic effects induced by different *Bothrops* venoms and isolated toxins<sup>20,21,31,33,34</sup>. By contrast, acetylsalicylic acid (ASA) is a largely used commercial drug with anti-inflammatory and analgesic activities<sup>35,36</sup>. ASA inhibited the catalytic activity of pancreatic PLA<sub>2</sub><sup>37</sup> but was not tested against the myotoxic effects induced by PLA<sub>2</sub>-like proteins from snake venom.

Thus, in the present work, three different techniques (myography, crystallography and bioinformatics assays) were used to test the potential inhibitory characteristics of two different ligands, acetylsalicylic acid (ASA) and rosmarinic acid (RA), against the PLA<sub>2</sub>-like myotoxin MjTX-II. In addition, these functional and structural experiments were used to obtain additional insight into the myotoxic mechanism of MjTX-II (and consequently of other PLA<sub>2</sub>-like myotoxins) and in the search for efficient inhibitors of PLA<sub>2</sub>-like proteins.

## Results

**Neuromuscular blocking activity.** *In vitro* myographic assays of the indirectly evoked contractions in nerve-muscle preparations has been a very sensitive model to functionally evaluate the myotoxic activity of PLA<sub>2</sub>-like toxins<sup>17–20,23,38–41</sup>. MjTX-II (1  $\mu$ M,  $N = 3$ ) promoted a time-dependent blockage of indirectly evoked twitches in mouse phrenic-diaphragm (PD) preparations. After 90 minutes, the twitch amplitudes were reduced by 92.6% (Fig. 1). The paralyzing effect of MjTX-II could not be reversed by washing the preparation for at least 30 minutes with toxin-free Ringer's physiological solution (data not shown). RA prevented approximately 87.3% of the muscle paralysis promoted by MjTX-II in 90 minutes when both were pre-incubated (at a toxin:inhibitor ratio of 1:1, w/w, i.e., 1:40, m/m;  $N = 3$ ) (Fig. 1a). However, ASA did not prevent the neuromuscular blockage in 90 minutes when MjTX-II and this compound were pre-incubated (at a toxin:drug ratio of 1:20, m/m;  $N = 3$ ) (Fig. 1b). Alone, RA (40  $\mu$ M,  $N = 3$ ) and ASA (20  $\mu$ M,  $N = 3$ ) did not affect the muscle contractions (Fig. 1).

**Crystallographic structures.** The crystal structures of both MjTX-II complexes present similar folding found in class-II PLA<sub>2</sub>s solved to date, including seven disulfide bridges in each protomer and the following structural features: an N-terminal  $\alpha$ -helix; a “short” helix; a Ca<sup>2+</sup> binding loop (non-functional for PLA<sub>2</sub>-like toxins); two  $\alpha$ -helices; two short strands of anti-parallel  $\beta$ -sheet ( $\beta$ -wing) and a C-terminal loop<sup>10,42</sup>.

The MjTX-II/RA crystal diffracted up to 1.60 Å and belonged to the P2<sub>1</sub>2<sub>1</sub>2<sub>1</sub> space group. The refinement converged to an R<sub>cryst</sub> of 15.7% (R<sub>free</sub> = 19.1%) with one RA molecule located close to the MDiS and helix 1 from monomer A and 392 water molecules (Table 1, Fig. 2a and b). Due to the lack of electron density, the side chains of the following residues were not modeled: Lys69 and Lys116 from monomer A and Lys70, Lys115, Lys128 and Lys129 from monomer B.

	MjTX-II/RA	MjTX-II/ASA
Space Group	P2 <sub>1</sub> 2 <sub>1</sub> 2 <sub>1</sub>	P2 <sub>1</sub>
Unit Cell (Å, °)	a = 46.1; b = 65.8; c = 90.4	a = 39.6; b = 65.6; c = 55.1; β = 92.7
Resolution range (Å)	23.55–1.59 (1.65–1.59)	18.32–1.69 (1.75–1.69)
Unique reflections	37011 (3613)	29552 (2767)
Multiplicity	9.7 (4.7)	3.3 (3.2)
Completeness (%)	99.7 (98.7)	94.0 (88.9)
Mean I/σ (I)	21.82 (3.0)	16.3 (2.4)
Molecules in ASU	2	2
Matthews coefficient V <sub>M</sub> (Å <sup>3</sup> Da <sup>-1</sup> )	2.5	2.5
R <sub>merge</sub> <sup>b</sup> (%)	10.5 (72.3)	4.9 (53.3)
Reflections used in refinement	37010 (3613)	29545 (2764)
Reflections used for R <sub>free</sub>	1851 (181)	1441 (129)
R <sub>work</sub>	15.8 (20.7)	17.9 (23.4)
R <sub>free</sub>	19.0 (23.7)	21.8 (28.7)
Number of non-hydrogen atoms		
Protein	1913	1908
Water	392	314
Ligands	26	38
Rosmarinic acid / CC	1/0.8	—
Acetylsalicylic acid / CC	—	2/0.8; 0.8
Average B-factor		
Overall	21.3	25.2
Protein	18.9	23.6
Ligands	35.4	39.1
Solvent	31.9	33.8
Ramachandran Plot (%) <sup>c</sup>		
Favored	97.1	96.7
Outliers	0	0
Rotamer outliers (%)	1.4	0
C <sub>β</sub> outliers	0	0
Clash score	3.17	6.84
RMS (bonds) (Å)	0.013	0.013
RMS (angles) (°)	1.57	1.16

**Table 1.** X-ray data collection and refinement statistics for MjTX-II/RA and MjTX-II/ASA structures. Numbers in parenthesis are for the highest resolution shell.

The MjTX-II/ASA crystal diffracted up to 1.69 Å resolution and belonged to the P2<sub>1</sub> space group. The final refined data converged to an R<sub>cryst</sub> of 18.1% (R<sub>free</sub> = 21.8%), with two ASA molecules interacting with the hydrophobic channel from each monomer, 3 DMSO molecules, and 314 water molecules (Table 1, Fig. 2c,d). Due to the lack of electron density, the side chains of Lys7, Lys60 and Lys117 residues from monomer A and Lys53, Lys69, Lys105 and Lys117 residues from monomer B are not modeled. Both crystal structures (coordinates and structure factors) were deposited into the Protein Data Bank (PDB) under the following ids: 6MQD (MjTX-II/RA) and 6MQF (MjTX-II/ASA).

The superposition between the PLA<sub>2</sub>-like myotoxins (*e.g.*, PrTX-I/RA, MjTX-II/FA14 and BthTX-I) and the structures solved here revealed that the MjTX-II/RA and MjTX-II/ASA structures present a distorted dimeric assembly (Fig. 3) as expressed by Euler angles<sup>15</sup> and center of mass displacement (COMdisp) values (see Methods section) (Table 2).

**Molecular dynamics.** The MD simulations of the MjTX-II/RA complex resulted in average RMS deviation of frame trajectories (ftRMSD) of the MjTX-II backbone atoms of 0.56 ± 0.11 nm (Fig. 4a) with no clear indication that the protein reached a stable conformation. The average RMS deviation of frame trajectories (ftRMSD) of the RA molecule was 0.22 ± 0.03 nm, indicating that the ligand interacts with the toxin in the same region (Fig. 4b). However, the RA effect on the MjTX-II quaternary structure results in its disturbance, forcing the toxin into a distorted conformation, evidenced by the increase of its radius of gyration (R<sub>g</sub>) from 20.0 to 21.8 Å and COMdisp of 31.5 Å (Table 2).

In contrast, MD simulation with the MjTX-II/ASA complex showed that the ASA molecules left their initial binding sites before 2 ns of the simulation, and subsequently, both molecules dissociated from MjTX-II or interacted non-specifically during the simulation. The unstable behavior of ASA can also be observed by the high standard deviation of ftRMSD value (0.51 ± 0.23 nm) (Fig. 4b). In addition, the MjTX-II/ASA complex did not

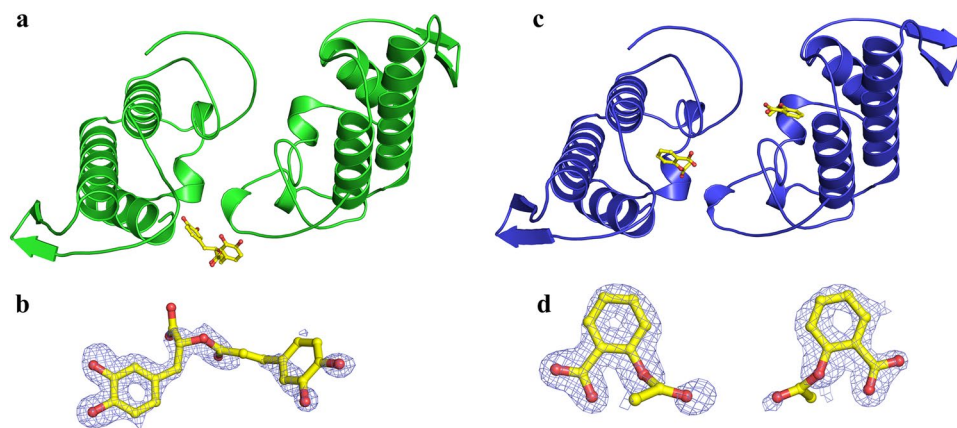


**Figure 2.** Crystal structures of MjTX-II/rosmarinic acid (RA) and MjTX-II/ acetylsalicylic acid (ASA) complexes. (a) The overall structure of the MjTX-II/RA complex is shown as a cartoon representation. The RA (yellow) molecule is illustrated as stick representation. (b) Omit electron density map (coefficients  $2|F_{\text{obs}}| - |F_{\text{calc}}|$ ) corresponding to RA is contoured at  $1.0\sigma$ . (c) The overall structure of the MjTX-II/ASA complex is shown as a cartoon representation. ASA (yellow) molecules are illustrated as stick representation. (d) Omit electron density map (coefficients  $2|F_{\text{obs}}| - |F_{\text{calc}}|$ ) corresponding to the ASA molecules bound to monomer A and B, respectively, are contoured at  $1.0\sigma$ .

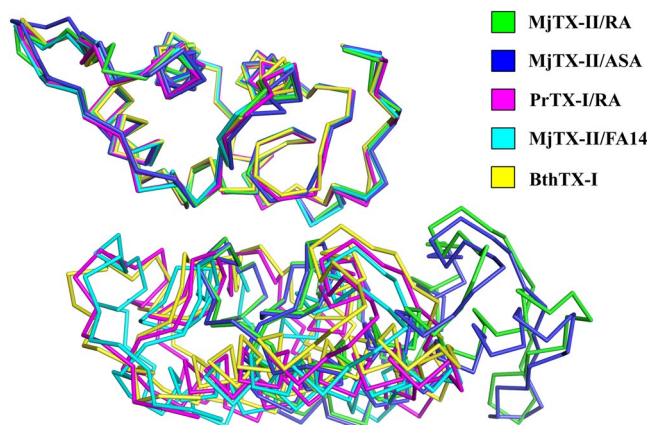


**Figure 3.** Superposition of  $C_{\alpha}$  atoms of one monomer from each of PLA<sub>2</sub>s-like structures: MjTX-II/RA (green), MjTX-II/ASA (blue), PrTX-I/RA (magenta), MjTX-II/FA14 (cyan) and BthTX-I (yellow) and the relative disposition of other monomers of each structure.

show a clear conformation stability during the simulation (Fig. 4a) and presented a ftRMSD backbone atoms of  $0.46 \pm 0.08$  nm.

In addition, other two MD simulations of 300 ns were performed aiming to test the dynamics of the distorted quaternary conformation observed in the MjTX-II/ASA complex, using the following systems: i) unbound MjTX-II and ii) unbound MjTX-II with fatty acid (FA) molecules (supposedly an activator PLA<sub>2</sub>-like myotoxin)<sup>14</sup>. FA molecules (stearic acids) were placed in the hydrophobic channel of this structure in a similar position as observed in the MjTX-II/stearic acid crystal structure (1XXS)<sup>43</sup>. The MD simulation of the unbound MjTX-II presented a high ftRMSD ( $0.64 \pm 0.11$  nm) (Fig. 4c) and an increase of its radius of gyration (Fig. 4d) compared with the active MjTX-II structure (MjTX-II/FA14)<sup>18</sup> (Table 2 and Fig. 5a). In contrast, MD simulation of the MjTX-II/FA presented more stability (ftRMSD of  $0.43 \pm 0.04$  nm) (Fig. 4c) and the model became more globular than its initial structure (see  $R_g$  in Table 2 and Fig. 4d), similar to the active structure<sup>18</sup>.

As observed in the Table 2, different parameters (e.g. COMdisp and  $R_g$ ) indicated that after MD simulation, the MjTX-II/FA complex had a conformation more similar with the active form (MjTX-II/FA14) and presented a more compact structure. The Fig. 5b shows the superposition between the MjTX-II/FA structure after the simulation and the active MjTX-II/FA14 crystal structure. In the Table 2, it is also possible to observe that the MjTX-II/FA complex may reach, for example at 170 ns of the MD simulation, a even more compact conformation which its  $R_g$  is very similar with the active MjTX-II/FA14 crystal structure ( $\sim 18$  Å). In addition, at this MD simulation moment the MjTX-II/FA complex presented a COMdisp decrease from 12.7 to 6.2 Å.

PDB id	Toxin	Roll (°)	Twist (°)	Tilt (°)	COMdisp (Å)	R <sub>g</sub> (Å)
3IQ3	BthTX-I/PEG4K	178	28	27	2.5	18.1
4K06	MTX-II/PEG4K	178	28	27	3.0	18.3
3QNL	PrTX-I/RA	173	24	34	1.7	18.5
6B84	apo-MjTX-II	164	22	73	7.9	18.7
6B81	MjTX-II/FA8	167	24	59	4.0	18.5
6B80	MjTX-II/FA14	170	21	51	0.0	18.5
6MQF	MjTX-II/ASA*	165	36	41	12.7	20.1
6MQD	MjTX-II/RA	166	35	47	13.3	20.0
-#	MjTX-II/RA	198	62	67	31.5	21.8
-#	MjTX-II/ASA	130	7	38	3.3	20.1
-#	Unbound MjTX-II	167	6	12	9.7	20.5
-#	MjTX-II/FA	178	32	40	11.2	19.5
-#	MjTX-II/FA <sup>§</sup>	179	42	33	6.2	18.7

**Table 2.** Calculated angles<sup>15</sup>, center of mass displacement (COMdisp) and radius of gyration (R<sub>g</sub>) for MjTX-II/RA, MjTX-II/ASA and other PLA<sub>2</sub>-like toxins quaternary structures. #Structures from molecular dynamics (MD) simulations. \*Reference structure for unbound MjTX-II and MjTX-II/FA MD simulation models. §MD simulation at frame 170 ns.

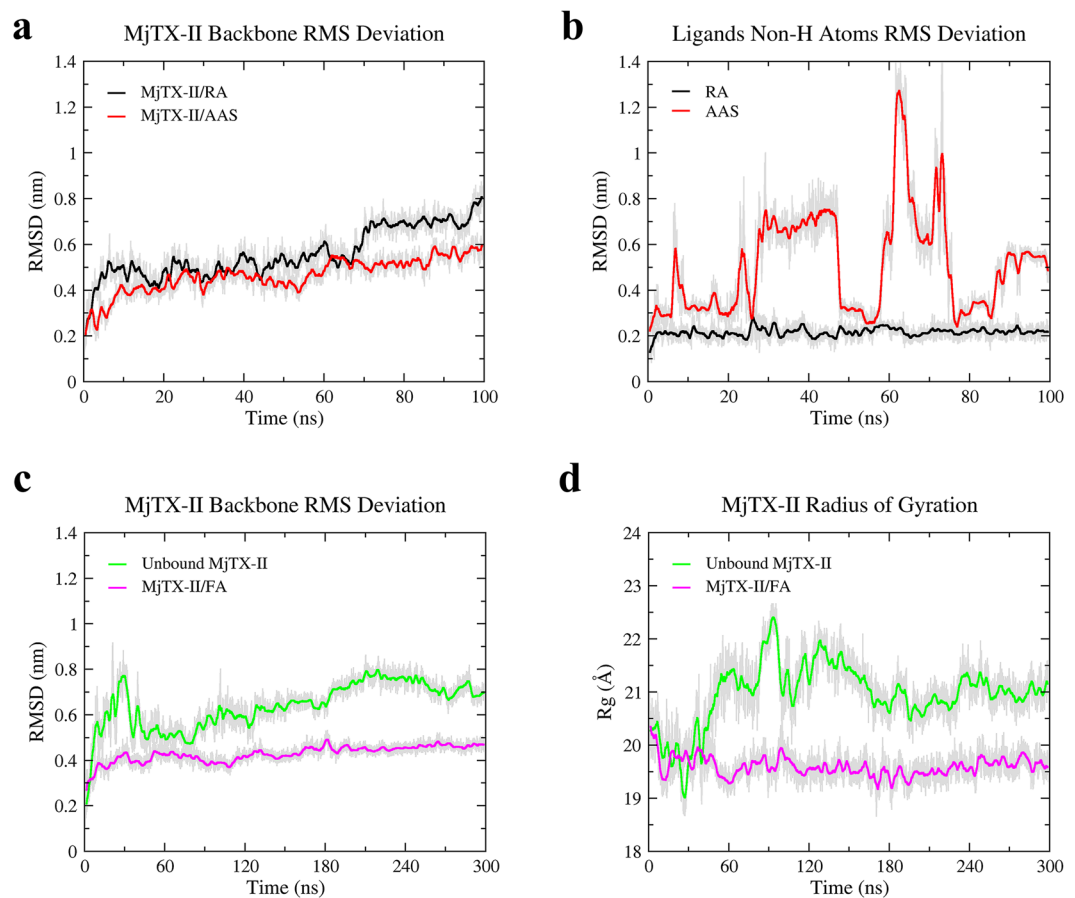


**Figure 4.** Molecular dynamics simulations with MjTX-II complexes. (a) Backbone atoms RMSD for MjTX-II/RA and MjTX-II/ASA complexes (black line for MjTX-II/RA and red line for MjTX-II/ASA). (b) Non-H atoms RMSD for RA and ASA ligands (black line - RA and red line - ASA molecules). (c) Backbone atoms RMSD for unbound MjTX-II (green) and MjTX-II/FA (magenta) complexes. (d) Radius of gyration (R<sub>g</sub>) for unbound MjTX-II (green) and MjTX-II/FA (magenta) complexes.

## Discussion

**Functional tests and inhibition efficiency of the ligands.** Similar to other PLA<sub>2</sub>-like proteins, MjTX-II can induce the blockage of twitches in mouse PD preparations using indirect and direct stimuli<sup>17,20,40,41,44–48</sup>. This paralyzing activity promoted by PLA<sub>2</sub>-like proteins has been proposed to result from the destabilization of the

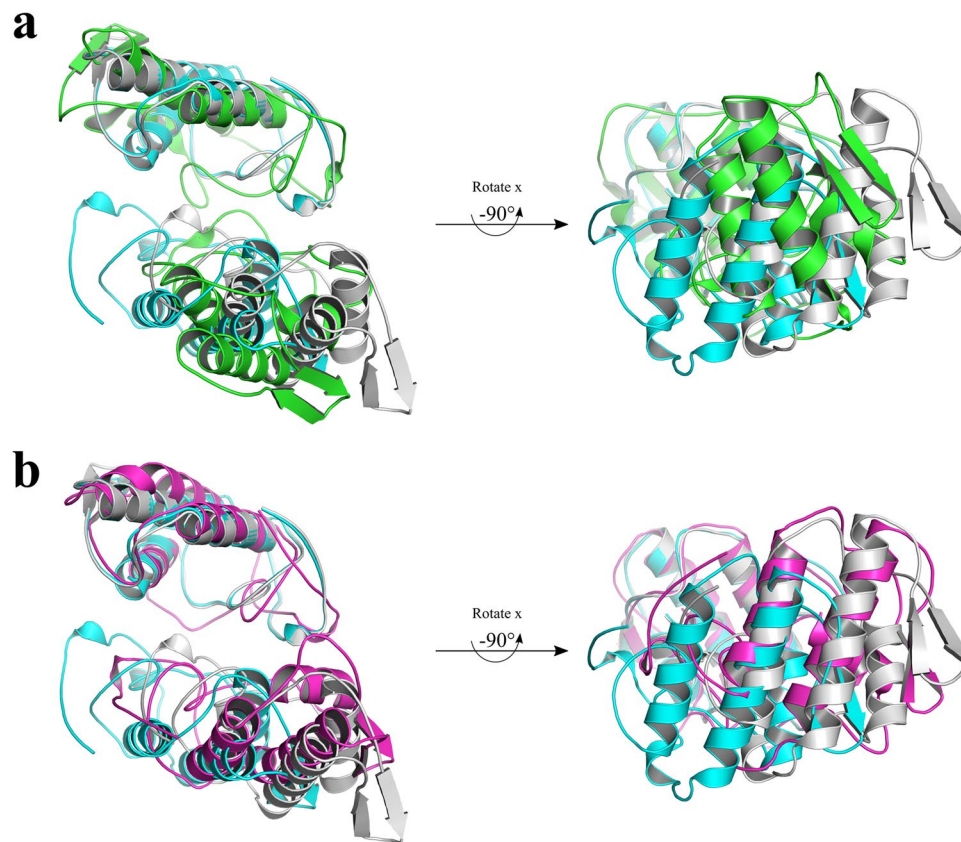


**Figure 5.** Superposition of the active MjTX-II crystal structure (MjTX-II/FA14, PDB id: 6B80) and structures from MD simulations. **(a)** Superposition between MjTX-II/FA14 crystal structure (cyan), the unbound MjTX-II model before (gray) and after (green) the MD simulation. **(b)** Superposition between MjTX-II/FA14 crystal structure (cyan), the MjTX-II/FA model before (gray) and after (magenta) the MD simulation.

muscle membrane<sup>38</sup>. Initially, this membrane disarrangement results in the loss of permeability control to ions and macromolecules<sup>49–51</sup>. Thus, there is cellular depolarization, including the re-equilibrium of  $\text{Na}^+$ ,  $\text{K}^+$  and  $\text{Cl}^-$  ions<sup>38,49,52</sup>, the influx of extracellular  $\text{Ca}^{2+}$  ions<sup>53,54</sup> and the release of intracellular  $\text{Ca}^{2+}$  ions<sup>55</sup>. Thus, an increase in the sarcoplasmic  $\text{Ca}^{2+}$  concentration promotes a series of adverse events, such as muscle contracture<sup>49</sup>, hypercontraction of myofilaments, mitochondrial damage and activation of proteases and  $\text{Ca}^{2+}$ -dependent  $\text{PLA}_2$ <sup>50,51</sup>, which amplifies the process of muscle injury<sup>52,53</sup>. Finally, the ATP released by the injured sarcolemma diffuses into neighboring regions of muscle fibers unaffected by the toxin, activating its P2X purinergic receptors in these muscle fibers with the consequent transmembrane passage of  $\text{Na}^+$ ,  $\text{K}^+$  and  $\text{Ca}^{2+}$  ions<sup>56–59</sup>. This ion movement results in the depolarization of these newly affected regions and an amplification of the muscle injury process in regions away from the initially disrupted sarcolemma.

Herein, we tested the ability of RA molecules to neutralize this destabilizing membrane activity through the paralyzing effect promoted by MjTX-II. Thus, we demonstrated that RA significantly reduces the blockage of indirectly evoked muscle induced by MjTX-II (Fig. 1), similarly to observed against PrTX-I, a  $\text{PLA}_2$ -like myotoxin from *Bothrops pirajai* venom<sup>20</sup>. Ticli and colleagues (2005), using different technical approaches, observed the antimyotoxic potential of RA against the crude venom of *Bothrops jararacussu* and against the main  $\text{PLA}_2$ -like myotoxins (BthTX-I and II) from this venom, as well the enhancement effect of serum therapy by this inhibitor. Furthermore, the authors exclude the proteolytic degradation of the toxin as a potential mechanism involved in the inhibition by RA<sup>21</sup>. Analogously, other molecules also presented an inhibitory effect against muscle paralysis promoted by  $\text{PLA}_2$ -like toxins, such as suramin against MjTX-II<sup>17</sup> and BthTX-I<sup>41</sup> and  $\text{Zn}^{2+}$  ions<sup>19</sup> and chicoric acid against BthTX-I<sup>23</sup>.

ASA is the most widely used drug in the world<sup>60</sup> and, since the 1970s, it has been known that mechanism of anti-inflammatory, analgesic and antipyretic activities by this molecule occurs through cyclooxygenase (COX) inhibition<sup>35,60</sup>. Furthermore, other studies have investigated different applications of ASA, including its action against whole venom from *Daboia russelii* (*Viperidae*)<sup>36</sup> and its toxic effects against catalytic  $\text{PLA}_2$ <sup>61–64</sup>. Singh and colleagues (2005) proposed the structural basis of an elapid  $\text{PLA}_2$  inhibition by ASA, but no functional assays were performed<sup>65</sup>. Recently, ASA was evaluated against the catalytic inhibitory activity of a pancreatic  $\text{PLA}_2$ <sup>37</sup> (a secreted  $\text{PLA}_2$  with similar activity to  $\text{PLA}_2$ s from *Viperidae* snake venom<sup>66</sup>) by bioinformatics and affinity assays. A weak interaction between ASA and the enzyme by affinity assays was observed, and a possible interaction at the  $\text{Ca}^{2+}$  binding loop was suggested by docking assays<sup>37</sup>. Thus, to test the ability of ASA to inhibit  $\text{PLA}_2$ -like toxins, we performed the first tests of its interaction with a  $\text{PLA}_2$ -like toxin and the physiological-pharmacological

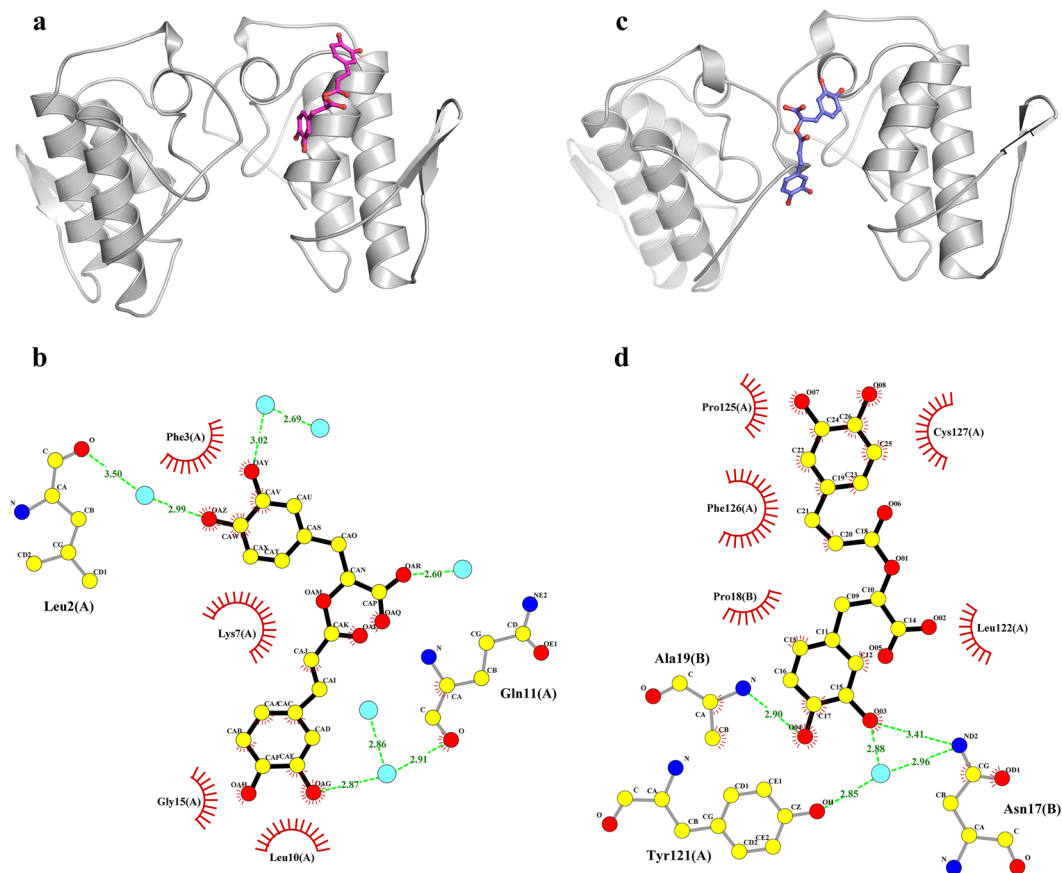


**Figure 6.** Comparison between MjTX-II/RA and PrTX-I/RA crystal structures. **(a)** Crystal structure of the PrTX-I/RA (PDB id: 3QNL) is shown as cartoon representation and RA inhibitor (magenta) is illustrated in stick representation. **(b)** Interaction of RA molecule in the PrTX-I structure. The representation of the interactions of RA was depicted as polar contacts (broken lines) and hydrophobic contacts (arcs with radiating spokes). Water molecules are shown as cyan spheres. **(c)** Crystal structure of the MjTX-II/RA is shown as cartoon representation and RA inhibitor (dark blue) is illustrated in stick representation. **(d)** Interaction of RA molecule in the MjTX-II structure. The representation of the interactions of RA was depicted as polar contacts (broken lines) and hydrophobic contacts (arcs with radiating spokes).

inhibition assays. Interestingly, despite the structural similarities between catalytic PLA<sub>2</sub> and myotoxic PLA<sub>2</sub>-like toxins (without catalytic activity), ASA did not inhibit the blockage of indirectly evoked muscle contractions promoted by MjTX-II (Fig. 1).

**Structural evidence for MjTX-II inhibition by rosmarinic acid.** To date, only one crystal structure of a PLA<sub>2</sub>-like/RA complex, PrTX-I/RA (PrTX-I from *B. pirajai* venom complexed to RA), has been deposited in the Protein Data Bank. In this structure, an inhibitor molecule interacts with the N-terminal residues of a toxin monomer<sup>20</sup> (Fig. 6a,b), and therefore, the RA molecule physically blocks the access of fatty acid molecules to the hydrophobic channels of PrTX-I. According to the current myotoxic mechanism proposed for PLA<sub>2</sub>-like toxins<sup>14,15</sup>, the entrance of a fatty acid (FA) molecule in the hydrophobic channel of the toxin is the first step of the molecular mechanism and leads to the allosteric activation of these toxins, with the subsequent exposure and alignment of their membrane docking and disruption sites (MDoS and MDiS, respectively). Thus, the RA molecule may prevent the activation of PrTX-I by blocking its hydrophobic channel.

Similar to the PrTX-I/RA complex, the crystal structure of the MjTX-II/RA complex revealed an inhibitor molecule interacting with the toxin; however, RA interacts with both monomers simultaneously and in a different region of MjTX-II (Fig. 6c). The first benzene ring region of the RA molecule (derived from the diphenyl-lactic acid portion) interacts with the N-terminus of monomer B (Asn17, Pro18 and Ala19 residues). The second benzene ring region of the RA molecule (derived from the caffeic acid portion) interacts with residues of the C-terminal region of monomer A (Leu122, Phe126 and Cys127 residues) (Fig. 6d), which includes the MDiS region.

Interestingly, RA and suramin<sup>17</sup> are efficient inhibitors for MjTX-II and other PLA<sub>2</sub>-like toxins (*e.g.*, BthTX-I, PrTX-I, MjTX-I, BaspTX-II and Ecarpholin S), but they bind to different regions of these toxins and display different inhibition mechanisms<sup>20–22,41,67</sup>. Furthermore, it is important to highlight that several structural studies with MjTX-II complexes<sup>16–18,43</sup> demonstrated that the binding of ligands in MjTX-II is always different when

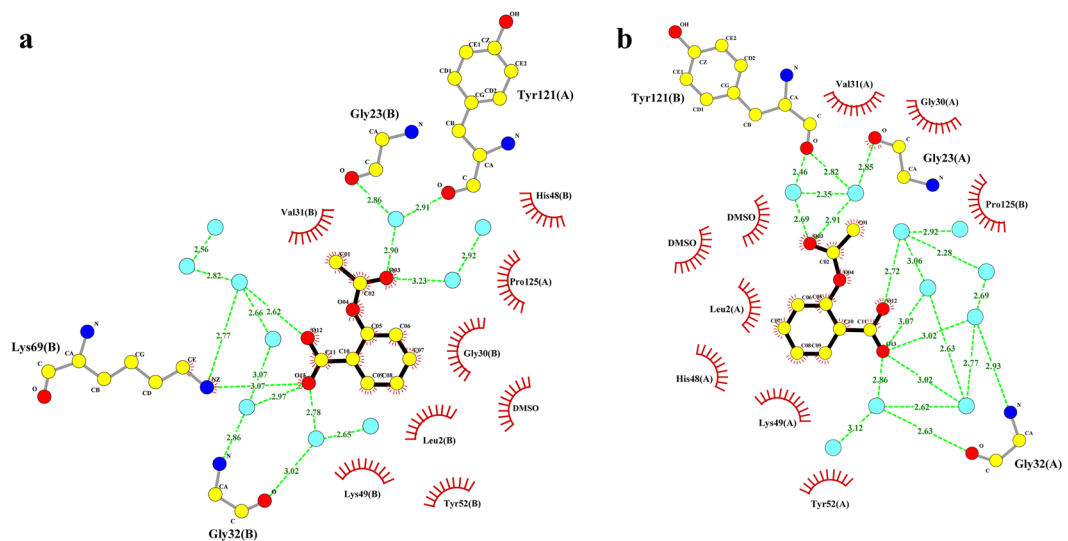


**Figure 7.** Interaction of ASA molecules with MjTX-II. ASA molecule interacting with hydrophobic channel residues from MjTX-II - monomer A (**a**) and monomer B (**b**). The representation of the interactions was depicted as polar contacts (broken lines) and hydrophobic contacts (arcs with radiating spokes). Water molecules are shown as cyan spheres.

compared to other PLA<sub>2</sub>-like toxins<sup>20,22,39,68</sup>. This fact was attributed to a residue insertion (Asn120) and two residue mutations (at positions 32 and 121), which cause the binding of additional ligands (*e.g.*, fatty acids or PEG) or interactions in different regions (RA and suramin).

Several functional/structural studies with PLA<sub>2</sub>-like toxins and ligands (*e.g.*, aristolochic and chicoric acids, suramin and Zn<sup>2+</sup> ions)<sup>17,19,23,39</sup> have demonstrated that their binding to the MDiS region is associated with the inhibition of these myotoxins, such as that observed in the crystal structure and functional data of the MjTX-II/RA complex presented here. Thus, an explanation of these phenomena is probably the lack of membrane disruption function of PLA<sub>2</sub>-like toxins.

**Acetylsalicylic acid binds to MjTX-II but does not inhibit its myotoxicity.** The crystal structure of the MjTX-II/ASA complex reveals that an ASA molecule is bound in the hydrophobic channel of each MjTX-II monomer. Thus, these two ASA ligands establish hydrophobic interactions with several residues, some of which are conserved from catalytic PLA<sub>2</sub>s, such as His48, Tyr52 and Gly30, and are essential for the coordination of co-factor Ca<sup>2+</sup> and for the catalytic activity of those enzymes<sup>10,69</sup>. Therefore, at first sight, the results may suggest that ASA inhibits PLA<sub>2</sub>-like toxins because its binding may prevent the activation of the toxin by fatty acid molecules (the first step of the proposed myotoxic mechanism). However, in the same functional experiments with PD preparations, as performed by myographic assays with MjTX-II/RA treatment, the inhibitory ability of ASA against the neuromuscular blockage induced by MjTX-II was not observed.

One explanation for these contrasting observations may be related to the low stability of the ASA molecules in the complex with the toxin, as observed in MD simulations (Fig. 4b) and due to the high content of water molecules mediating the interaction between the ligand and the toxin (Fig. 7). This eventual instability may lead to its displacement by FA molecules present in the isolated organ-bath chamber, promoting a return to the active form of MjTX-II<sup>18</sup>.

The presence of FA molecules in the chamber may be explained by the method employed in this assay<sup>70</sup>. During the removal of PD preparations from animals and their assembly in these chambers, PD preparations are sufficiently manipulated to cause initial lesions of some muscle fibers, disrupting their sarcolemma (composed of phospholipids, FA molecules and several other macromolecules) with the consequent release of their intracellular content. Although the PD preparation is subjected to washing procedures after its assembly and a stabilization period of the evoked contractions occurs before the beginning of the assays, the lesions remain in the PD preparations with continuous release of the intracellular content from injured fibers, including cytosolic phospholipases and other proteases that are activated by Ca<sup>2+</sup> ions<sup>50,51</sup>. Thus, apart from the remnants of FA molecules between the PD preparation washes, these cytosolic proteases can amplify the process of muscle injury<sup>52,53</sup>, releasing FA molecules prior to toxin addition into the chamber.

**MD simulations with MjTX-II/RA, MjTX-II/ASA and MjTX-II/FA shed light on the inhibition of the myotoxic mechanism.** Aiming to further understand the observations achieved with myographic and crystallographic methods in the present study, the dynamic of the inhibitory process was studied by MD simulations, and four different systems were considered: (i) MjTX-II/RA, (ii) MjTX-II/ASA, (iii) unbound MjTX-II and (iv) MjTX-II/FA, as described in the results section. Thus, we observed that (i) the RA molecule interacted with the toxin throughout the simulation and the toxin reaches a even more distorted quaternary structure (Fig. 4b); (ii) ASA molecules dissociated from MjTX-II at the beginning of the simulation (Fig. 4b), but the quaternary structure presented a reasonable conformational stability throughout the simulation (Fig. 4a); (iii) the removal

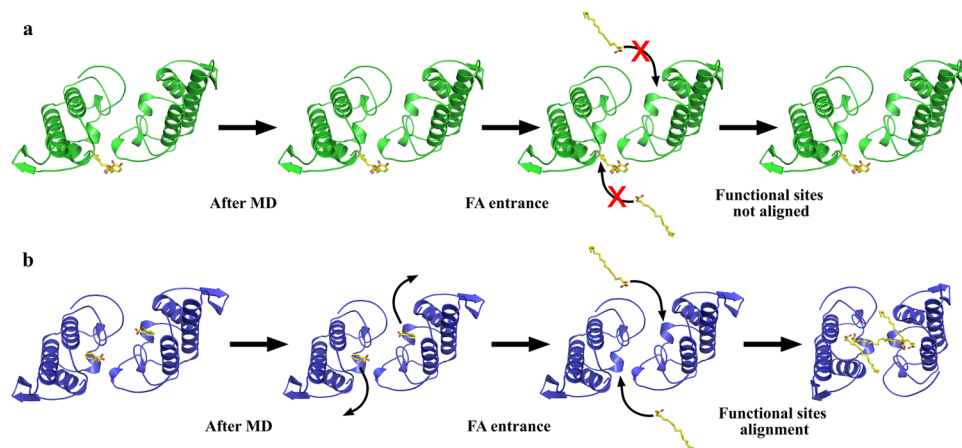


**Figure 8.** Schematic representation of structural changes caused by ligands. **(a)** In the MjTX-II/RA structure, the RA ligand is kept tight bound to the protein and blocks the interaction of fatty acids with the toxin, preventing the alignment of its functional sites. **(b)** In the MjTX-II/ASA structure, ASA ligands interact with low stability to the toxin, as observed in MD simulations, thus, fatty acids may bind with the toxin and, consequently, its functional sites may be exposed to the solvent.

of ligand molecules from the MjTX-II/ASA complex (unbound MjTX-II) was not sufficient to lead the complex to an undistorted conformation until the end of the simulation, as expected for the *apo*-MjTX-II structure<sup>18</sup> (Fig. 4c,d and Table 2); and (iv) in the presence of FA molecules, the quaternary structure of MjTX-II (starting from an initial distorted conformational MjTX-II/ASA model) became more globular and symmetric (Fig. 8).

Therefore, these findings highlight the efficiency of RA as inhibitor of the toxic effects promoted by MjTX-II as observed by functional methods. The results suggest that RA inhibits this toxin not only by blocking its MDiS residues in a monomer but also by distorting the quaternary structure of MjTX-II, leading to misalignment of the MDiS and MDoS regions from both monomers, which affects its myotoxic activity.

Moreover, the dissociation of ASA in the beginning of the MD simulation suggests low stability and/or affinity of the ligand in its binding site. This observation is compatible with functional assays that did not detect myotoxicity reduction or neutralization in its presence, as discussed in the previous sections.

FA molecules have an important role for oligomeric changes that lead to the activation of the myotoxic mechanism proposed for PLA<sub>2</sub>-like toxins<sup>14,15</sup>, but in the case of MjTX-II, their binding is not necessary for the alignment of the functional sites of this particular toxin<sup>18</sup>. However, the MD simulations performed here showed that the distorted starting model with no ligands (unbound MjTX-II) was not able to assume the active state (symmetric conformation), which may only obtain after the addition of FA molecules. These findings reinforce previous structural data with MjTX-II that showed that while FA molecules do not lead to important quaternary conformation changes, their binding has a direct influence on some side-chain orientations in the dimeric interface<sup>18</sup>, leading to stabilization of the dimeric conformation of MjTX-II.

## Conclusions

In the present study, functional, crystallographic and bioinformatics assays involving MjTX-II, a PLA<sub>2</sub>-like toxin with structural particularities, and two potential inhibitors were performed. RA, previously tested as an efficient inhibitor for a PLA<sub>2</sub>-like toxin (PrTX-I), was demonstrated to be highly efficient for the inhibition of MjTX-II in mouse PD preparations. Interestingly, despite similar inhibitory effects against MjTX-II and PrTX-I, the RA binding sites in these toxins are different. In the case of MjTX-II, the inhibitory effect is attributed to binding in the MDiS region, which prevents the disruptive activity of the toxin. In addition, the distorted quaternary conformation of MjTX-II after RA binding may also contribute to its inactivity. In contrast, ASA, a ligand previously tested in catalytic PLA<sub>2</sub>, was not able to prevent the paralyzing effect of MjTX-II, despite its binding in the MjTX-II/ASA crystal structure. The MD simulation with MjTX-II/ASA showed the low stability of this ligand in the hydrophobic channel of MjTX-II, suggesting that this molecule may be replaced with another molecule with higher affinity (such as fatty acids) in the functional assays, which can then activate the toxin. Finally, MD simulations of a MjTX-II/FA model led to a symmetric and stable structure, which reinforces the importance of fatty acids for the stabilization of the toxin. This combination of functional, structural and bioinformatics assays used here can methodologically contribute to the design of effective antiophidic molecules.

## Experimental Procedures

**Toxin isolation and ligands source.** Freeze-dried crude venom (150 mg) was solubilized in 0.05 M ammonium bicarbonate pH 8.0 and subjected to ion exchange chromatography. The fraction corresponding to MjTX-II was obtained by a gradient of 0.05 to 0.5 M ammonium bicarbonate pH 8.0, as described by Soares and colleagues<sup>71</sup>. For contaminant removal, this fraction was subjected to reversed-phase chromatography, with a gradient of 0–66.5% acetonitrile (in 0.1% trifluoroacetic acid) in a C18 column (Shimadzu). Acetylsalicylic acid (ASA) and rosmarinic acid (RA) were purchased from Sigma-Aldrich, St. Louis, Missouri, USA.

**Functional studies.** Adult male mice (25–30 g) were euthanized by exsanguination after cervical dislocation to remove the phrenic nerve-diaphragm muscle and mounted vertically (under a resting tension of 5 g) in a conventional isolated organ-bath chamber containing 15 mL of physiological solution (135 mM NaCl, 5 mM KCl, 1 mM MgCl<sub>2</sub>, 2 mM CaCl<sub>2</sub>, 15 mM NaHCO<sub>3</sub>, 1 mM Na<sub>2</sub>HPO<sub>4</sub> and 11 mM glucose). This solution was constantly bubbled with carbogen (95% O<sub>2</sub> and 5% CO<sub>2</sub>) and maintained at 35 ± 2 °C. The phrenic-diaphragm (PD) preparation was attached to an isometric force transducer (Grass-Telefactor, FT03) for recording twitch tension. The transducer signal output was amplified and recorded on a computer, via a transducer signal conditioner (Gould Systems, 13-6615-50), with the AcquireLab Data Acquisition System (Gould). Indirect contractions were evoked by rectangular pulses (0.2 Hz, 0.5 ms) and a supramaximal intensity delivered from an electronic stimulator (Grass-Telefactor, S88K) and applied to the phrenic nerve by means of a suction electrode.

Preparations were stabilized for 45 minutes before the treatment. For inhibition experiments, 1 μM MjTX-II dissolved in Ringer's physiological solution was mixed with RA and ASA at a 1:10 and 1:20 (m/m) toxin:drug ratio, respectively. Mixtures were incubated for 30 minutes at 35 °C (± 2 °C). Control experiments were performed in the absence of toxin and in the presence of RA (10 μM) or ASA (20 μM) alone. The results are expressed as the mean ± S.E. Data were analyzed by ANOVA complemented with the Tukey-Kramer test. Values of  $P < 0.05$  were considered significant.

The animals were supplied by UNESP (Biotério Central da Universidade Estadual Paulista, Botucatu, SP, Brazil). The Institutional Animal Care and Use Committee (Institute of Biosciences - São Paulo State University - UNESP) approved this study (number 033/05). The animal procedures were performed in accordance with the guidelines prepared by the Committee on the Care and Use of Laboratory Animal Resources, National Research Council, USA.

**Crystallization and X-ray data collection.** The purified fraction of MjTX-II used for co-crystallization was concentrated up to 10 mg.mL<sup>-1</sup> and solubilized in 20 mM ammonium bicarbonate, pH 8.0. ASA was dissolved in 100% dimethyl sulfoxide (DMSO) and RA was dissolved in 95% ammonium bicarbonate (20 mM, pH 8.0) and 5% ethanol to obtain a molar ratio of 1:8 (protein:ligand, for both compounds) in crystallization drops. Crystals from MjTX-II/RA and MjTX-II/ASA complexes were obtained by a conventional hanging drop vapor-diffusion method<sup>72</sup> at constant temperature of 291 K for approximately 20 days, from a mixture of 1 μL of protein/inhibitor solution (previously incubated for 30 minutes) and 1 μL of reservoir solution and equilibrated against a reservoir (500 μL). The reservoir solution was similar to that previously found in the literature for this toxin and was composed of PEG 4000, Tris HCl pH 8.5 and lithium sulfate (MjTX-II/RA) and PEG 4000, isopropanol and sodium citrate (MjTX-II/ASA)<sup>16–18</sup>.

The crystals were mounted in a nylon loop and flash-cooled in a stream of liquid nitrogen using no cryoprotectant for X-ray diffraction data collection. The datasets were obtained using a synchrotron radiation source (MX2 station, Laboratório Nacional de Luz Sincrotron (LNLS), Campinas, Brazil) and a PILATUS 2 M detector (Dectris) at a wavelength of 1.458 Å (at 100 K).

**Structure determination and refinement.** The dataset corresponding to MjTX-II/RA was processed using the HKL2000 v.1.8.4 software package<sup>73</sup>, and the MjTX-II/ASA dataset was processed using AutoPROC v.1.0.5 software<sup>74</sup>.

Both crystal structures were solved by the Molecular Replacement Method using the software PHASER<sup>75</sup> from PHENIX software package v.1.12<sup>76</sup> and the monomer A atom coordinates of MjTX-II/FA14 (PDB access code 6B80) as a search model. The modeling, ligand insertion, solvent molecules and manual refinement process were performed using Coot v.0.8.9 software<sup>77</sup>. Structural automated refinement of models was performed by PHENIX software package v.1.12<sup>76</sup>, and the structural quality was checked using PHENIX software package v.1.12 and MolProbity software<sup>78</sup>.

**Structural comparative analysis.** For the structural comparisons, the structures of MjTX-II/RA and MjTX-II/ASA (this work), *apo*-MjTX-II (PDB id: 6B84), MjTX-II/FA8 (PDB id: 6B81), MjTX-II/FA14 (PDB id: 6B80)<sup>18</sup>, MjTX-II/PEG4K (PDB id: 4KF3)<sup>16</sup> and PrTX-I/RA (Piratoxin-I from *Bothrops pirajai* - PDB id: 3QNL)<sup>20</sup> were used. Molecular comparison of the structures was performed using Coot v.0.8.9 software<sup>77</sup>. All structural figures was generated using PyMOL v.1.3 software<sup>79</sup> and LigPlot<sup>+</sup> v.1.4.5<sup>80</sup>.

In order to analyze the conformations, the center of mass (COM) displacement measure was calculated. This measurement considers the active MjTX-II structure (MjTX-II /FA14, PDB id: 6B80) as reference. For each subset the structures (Table 2), both monomers A were superposed (C<sub>α</sub> atoms) and COM was calculated for each monomers B; subsequently, the COM distance between both monomers B was calculated by Euclidean distance, resulting in a displacement value called COMdisp.

**Molecular dynamics (MD) simulation.** All MD simulations were performed using GROMACS (Groningen Machine for Chemical Simulation) v.5.0.5<sup>81</sup> under GROMOS96 54a7 force field<sup>82</sup>. MjTX-II protonation states were set to pH 8.0 using PROPKA3 server<sup>83</sup>, and each complex was placed in a triclinic box. The systems were solvated using simple point charge (SPC) water models to maintain the crystallographic water molecule positions and were equilibrated with 100 mM NaCl. A minimization step was applied using the Steepest Descent algorithm to reach a system energy below 100 kJ/mol/nm, and then, MjTX-II, RA, ASA and FA were restrained to perform an 1 ns NVT step using a V-rescale thermostat<sup>84</sup> at 310 K followed by an 1 ns NPT step adding Berendsen barostat<sup>85</sup> at 1 bar to accommodate the systems. Furthermore, unrestrained MD simulations were performed for each system using a Nose-Hoover thermostat<sup>86,87</sup> and Parrinello-Rahman barostat<sup>88</sup>.

MD simulations of 100 ns were performed using the MjTX-II/ASA and MjTX-II/RA crystallographic structures. MD simulations of 300 ns were performed using MjTX-II/ASA crystal structure, only removing ASA

molecules (unbound MjTX-II system), or removing ASA molecules and adding stearic acid molecules in each hydrophobic channel (MjTX-II/FA system). Stearic acid molecules were added manually, based on the crystallographic structure of MjTX-II complexed with stearic acid (PDB id: 1XXS)<sup>43</sup> using Coot v.0.8.9 software<sup>77</sup>.

RA, ASA and FA topologies were built using the online server Automated Topology Builder (ATB) v.2.2 (<https://atb.uq.edu.au/>)<sup>89</sup>, which uses Quantum Mechanics calculations to determine bonded and non-bonded information, while charges were manually corrected to harmonize with force field parameters.

## References

- Otero, R. *et al.* Complications of *Bothrops*, *Porthidium*, and *Bothriechis* snakebites in Colombia. A clinical and epidemiological study of 39 cases attended in a university hospital. *Toxicon* **40**, 1107–1114 (2002).
- Warrell, D. A. Snake bite. *Lancet* **375**, 77–88 (2010).
- Gutierrez, J. M., Theakston, R. D. & Warrell, D. A. Confronting the neglected problem of snake bite envenoming: the need for a global partnership. *PLoS Med* **3**, e150 (2006).
- Kasturiratne, A. *et al.* The global burden of snakebite: a literature analysis and modelling based on regional estimates of envenoming and deaths. *PLoS Med* **5**, e218 (2008).
- Gutierrez, J. M. *et al.* Neutralization of local tissue damage induced by *Bothrops asper* (terciopelo) snake venom. *Toxicon* **36**, 1529–1538 (1998).
- Lomonte, B., Angulo, Y. & Calderon, L. An overview of lysine-49 phospholipase A<sub>2</sub> myotoxins from crotalid snake venoms and their structural determinants of myotoxic action. *Toxicon* **42**, 885–901 (2003).
- Calvete, J. J. *et al.* Snake venomomics and antivenomics of *Bothrops colombiensis*, a medically important pitviper of the *Bothrops atrox-asper* complex endemic to Venezuela: Contributing to its taxonomy and snakebite management. *J Proteomics* **72**, 227–240 (2009).
- Ghazaryan, N. A. *et al.* Phospholipases A<sub>2</sub> from Viperidae snakes: Differences in membranotropic activity between enzymatically active toxin and its inactive isoforms. *Biochim Biophys Acta* **1848**, 463–468 (2015).
- Gutierrez, J. M. & Lomonte, B. Phospholipases A<sub>2</sub>: unveiling the secrets of a functionally versatile group of snake venom toxins. *Toxicon* **62**, 27–39 (2013).
- Arni, R. K. & Ward, R. J. Phospholipase A<sub>2</sub> - a structural review. *Toxicon* **34**, 827–841 (1996).
- dos Santos, J. I., Soares, A. M. & Fontes, M. R. Comparative structural studies on Lys49-phospholipases A<sub>2</sub> from *Bothrops* genus reveal their myotoxic site. *J Struct Biol* **167**, 106–116 (2009).
- Kini, R. M. Excitement ahead: structure, function and mechanism of snake venom phospholipase A<sub>2</sub> enzymes. *Toxicon* **42**, 827–840 (2003).
- Fernandes, C. A. *et al.* Structural bases for a complete myotoxic mechanism: crystal structures of two non-catalytic phospholipases A<sub>2</sub>-like from *Bothrops brazili* venom. *Biochim Biophys Acta* **1834**, 2772–2781 (2013).
- Fernandes, C. A., Borges, R. J., Lomonte, B. & Fontes, M. R. A structure-based proposal for a comprehensive myotoxic mechanism of phospholipase A<sub>2</sub>-like proteins from viperid snake venoms. *Biochim Biophys Acta* **1844**, 2265–2276 (2014).
- Borges, R. J., Lemke, N. & Fontes, M. R. M. PLA<sub>2</sub>-like proteins myotoxic mechanism: a dynamic model description. *Sci Rep* **7**, 15514 (2017).
- Salvador, G. H. *et al.* Structural and functional studies with myotoxin II from *Bothrops moojeni* reveal remarkable similarities and differences compared to other catalytically inactive phospholipases A<sub>2</sub>-like. *Toxicon* **72**, 52–63 (2013).
- Salvador, G. H. *et al.* Structural and functional evidence for membrane docking and disruption sites on phospholipase A<sub>2</sub>-like proteins revealed by complexation with the inhibitor suramin. *Acta Crystallogr D Biol Crystallogr* **71**, 2066–2078 (2015).
- Salvador, G. H. M., Dos Santos, J. I., Borges, R. J. & Fontes, M. R. M. Structural evidence for a fatty acid-independent myotoxic mechanism for a phospholipase A<sub>2</sub>-like toxin. *Biochim Biophys Acta* **1866**, 473–481 (2018).
- Borges, R. J. *et al.* Functional and structural studies of a Phospholipase A<sub>2</sub>-like protein complexed to zinc ions: Insights on its myotoxicity and inhibition mechanism. *Biochim Biophys Acta* **1861**, 3199–3209 (2017).
- Dos Santos, J. I. *et al.* Structural and functional studies of a bothropic myotoxin complexed to rosmarinic acid: new insights into Lys49-PLA<sub>2</sub> inhibition. *PLoS One* **6**, e28521 (2011).
- Ticli, F. K. *et al.* Rosmarinic acid, a new snake venom phospholipase A<sub>2</sub> inhibitor from *Cordia verbenacea* (Boraginaceae): antiserum action potentiation and molecular interaction. *Toxicon* **46**, 318–327 (2005).
- Murakami, M. T. *et al.* Inhibition of myotoxic activity of *Bothrops asper* myotoxin II by the anti-trypanosomal drug suramin. *J Mol Biol* **350**, 416–426 (2005).
- Cardoso, F. F. *et al.* Structural basis of phospholipase A<sub>2</sub>-like myotoxin inhibition by chicoric acid, a novel potent inhibitor of ophioid toxins. *Biochim Biophys Acta Gen Subj* **1862**, 2728–2737 (2018).
- Mendes, M. M. *et al.* Triacetyl p-coumarate: an inhibitor of snake venom metalloproteinases. *Phytochemistry* **86**, 72–82 (2013).
- Baraldi, P. T. *et al.* A novel synthetic quinolinone inhibitor presents proteolytic and hemorrhagic inhibitory activities against snake venom metalloproteases. *Biochimie* **121**, 179–188 (2016).
- Soares, A. M. *et al.* Medicinal plants with inhibitory properties against snake venoms. *Curr Med Chem* **12**, 2625–2641 (2005).
- Marcussi, S. *et al.* Snake venom phospholipase A<sub>2</sub> inhibitors: medicinal chemistry and therapeutic potential. *Curr Top Med Chem* **7**, 743–756 (2007).
- Carvalho, B. M. *et al.* Snake venom PLA<sub>2</sub>s inhibitors isolated from Brazilian plants: synthetic and natural molecules. *Biomed Res Int* **2013**, 153045 (2013).
- Hage-Melim, L. I., Sampaio, S. V., Taft, C. A. & Silva, C. H. Phospholipase A<sub>2</sub> inhibitors isolated from medicinal plants: alternative treatment against snakebites. *Mini Rev Med Chem* **13**, 1348–1356 (2013).
- Guimaraes, C. L. *et al.* Biodiversity as a source of bioactive compounds against snakebites. *Curr Med Chem* **21**, 2952–2979 (2014).
- Aung, H. T., Furukawa, T., Nikai, T., Niwa, M. & Takaya, Y. Contribution of cinnamic acid analogues in rosmarinic acid to inhibition of snake venom induced hemorrhage. *Bioorg Med Chem* **19**, 2392–2396 (2011).
- Petersen, M. & Simmonds, M. S. Rosmarinic acid. *Phytochemistry* **62**, 121–125 (2003).
- Aung, H. T., Nikai, T., Niwa, M. & Takaya, Y. Rosmarinic acid in *Argusia argentea* inhibits snake venom-induced hemorrhage. *J Nat Med* **64**, 482–486 (2010).
- Aung, H. T. *et al.* Biological and pathological studies of rosmarinic acid as an inhibitor of hemorrhagic *Trimeresurus flavoviridis* (habu) venom. *Toxins (Basel)* **2**, 2478–2489 (2010).
- Vane, J. R. Inhibition of prostaglandin synthesis as a mechanism of action for aspirin-like drugs. *Nat New Biol* **231**, 232–235 (1971).
- Wu, R. C., Chou, P. T. & Chen, L. K. Aspirin plus tirofiban inhibit the thrombosis induced by Russell's viper venom. *Thromb J* **14**, 38 (2016).
- Dileep, K. V. *et al.* Comparative studies on the inhibitory activities of selected benzoic acid derivatives against secretory phospholipase A<sub>2</sub>, a key enzyme involved in the inflammatory pathway. *Mol Biosyst* **11**, 1973–1979 (2015).
- Gallacci, M. & Cavalcante, W. L. Understanding the *in vitro* neuromuscular activity of snake venom Lys49 phospholipase A<sub>2</sub> homologues. *Toxicon* **55**, 1–11 (2010).
- Fernandes, C. A. *et al.* Structural Basis for the Inhibition of a Phospholipase A<sub>2</sub>-Like Toxin by Caffeic and Aristolochic Acids. *PLoS One* **10**, e0133370 (2015).

40. Cavalcante, W. L. *et al.* Neutralization of snake venom phospholipase A<sub>2</sub> toxins by aqueous extract of *Casearia sylvestris* (Flacourtiaceae) in mouse neuromuscular preparation. *J Ethnopharmacol* **112**, 490–497 (2007).
41. de Oliveira, M. *et al.* Antagonism of myotoxic and paralyzing activities of bothropstoxin-I by suramin. *Toxicon* **42**, 373–379 (2003).
42. Magro, A. J., Fernandes, C. A., dos Santos, J. I. & Fontes, M. R. Influence of quaternary conformation on the biological activities of the Asp49-phospholipases A<sub>2</sub>s from snake venoms. *Protein Pept Lett* **16**, 852–859 (2009).
43. Watanabe, L., Soares, A. M., Ward, R. J., Fontes, M. R. & Arni, R. K. Structural insights for fatty acid binding in a Lys49-phospholipase A<sub>2</sub>: crystal structure of myotoxin II from *Bothrops moojeni* complexed with stearic acid. *Biochimie* **87**, 161–167 (2005).
44. Gallacci, M., Oliveira, M., Dal Pai-Silva, M., Cavalcante, W. L. & Spencer, P. J. Paralyzing and myotoxic effects of a recombinant bothropstoxin-I (BthTX-I) on mouse neuromuscular preparations. *Exp Toxicol Pathol* **57**, 239–245 (2006).
45. Heluany, N. F., Homs-Brandeburgo, M. I., Giglio, J. R., Prado-Franceschi, J. & Rodrigues-Simioni, L. Effects induced by bothropstoxin, a component from *Bothrops jararacussu* snake venom, on mouse and chick muscle preparations. *Toxicon* **30**, 1203–1210 (1992).
46. Oshima-Franco, Y. *et al.* The presynaptic activity of bothropstoxin-I, a myotoxin from *Bothrops jararacussu* snake venom. *Basic Clin Pharmacol Toxicol* **95**, 175–182 (2004).
47. Ponce-Soto, L. A. *et al.* Neuromuscular activity of BaTX, a presynaptic basic PLA<sub>2</sub> isolated from *Bothrops alternatus* snake venom. *Comparative Biochemistry and Physiology C-Toxicology & Pharmacology* **150**, 291–297 (2009).
48. Stabeli, R. G. *et al.* *Bothrops moojeni* myotoxin-II, a Lys49-phospholipase A<sub>2</sub> homologue: an example of function versatility of snake venom proteins. *Comp Biochem Physiol C Toxicol Pharmacol* **142**, 371–381 (2006).
49. Rodrigues-Simioni, L., Borgese, N. & Ceccarelli, B. The effects of *Bothrops jararacussu* venom and its components on frog nerve-muscle preparation. *Neuroscience* **10**, 475–489 (1983).
50. Gutierrez, J. M. & Lomonte, B. Phospholipase A<sub>2</sub> myotoxins from *Bothrops* snake venoms. *Toxicon* **33**, 1405–1424 (1995).
51. Ownby, C. L., Selistre de Araujo, H. S., White, S. P. & Fletcher, J. E. Lysine 49 phospholipase A<sub>2</sub> proteins. *Toxicon* **37**, 411–445 (1999).
52. Montecucco, C., Gutierrez, J. M. & Lomonte, B. Cellular pathology induced by snake venom phospholipase A<sub>2</sub> myotoxins and neurotoxins: common aspects of their mechanisms of action. *Cell Mol Life Sci* **65**, 2897–2912 (2008).
53. Gutierrez, J. M. & Ownby, C. L. Skeletal muscle degeneration induced by venom phospholipases A<sub>2</sub>: insights into the mechanisms of local and systemic myotoxicity. *Toxicon* **42**, 915–931 (2003).
54. Villalobos, J. C., Mora, R., Lomonte, B., Gutierrez, J. M. & Angulo, Y. Cytotoxicity induced in myotubes by a Lys49 phospholipase A<sub>2</sub> homologue from the venom of the snake *Bothrops asper*: evidence of rapid plasma membrane damage and a dual role for extracellular calcium. *Toxicol In Vitro* **21**, 1382–1389 (2007).
55. Johnson, E. K. & Ownby, C. L. The role of extracellular ions in the pathogenesis of myonecrosis induced by a myotoxin isolated from Broad-Banded copperhead (*Agkistrodon contortrix laticinctus*) venom. *Comp Biochem Physiol Pharmacol Toxicol Endocrinol* **107**, 359–366 (1994).
56. Burnstock, G. Physiology and pathophysiology of purinergic neurotransmission. *Physiol Rev* **87**, 659–797 (2007).
57. Di Virgilio, F. Liaisons dangereuses: P2X<sub>7</sub> and the inflammasome. *Trends Pharmacol Sci* **28**, 465–472 (2007).
58. Abbracchio, M. P., Burnstock, G., Verkhratsky, A. & Zimmermann, H. Purinergic signalling in the nervous system: an overview. *Trends Neurosci* **32**, 19–29 (2009).
59. Cintra-Francischinelli, M. *et al.* *Bothrops* snake myotoxins induce a large efflux of ATP and potassium with spreading of cell damage and pain. *Proc Natl Acad Sci USA* **107**, 14140–14145 (2010).
60. Vane, J. R. & Botting, R. M. The mechanism of action of aspirin. *Thromb Res* **110**, 255–258 (2003).
61. Wang, J. P. & Teng, C. M. Comparison of the enzymatic and edema-producing activities of two venom phospholipase A<sub>2</sub> enzymes. *Eur J Pharmacol* **190**, 347–354 (1990).
62. Wang, J. P. & Teng, C. M. Effects of anti-inflammatory drugs on rat hind-paw swelling caused by phospholipase A<sub>2</sub> from *Naja naja atra* venom. *Naunyn Schmiedebergs Arch Pharmacol* **344**, 377–381 (1991).
63. Wang, J. P. & Teng, C. M. Roles of PMN leucocytes, platelets and some mediators in rat hind-paw oedema induced by two phospholipase A<sub>2</sub> enzymes from *Trimeresurus mucrosquamatus* venom. *J Pharm Pharmacol* **44**, 300–305 (1992).
64. Lobo, I. B. & Hoult, J. R. Groups I, II and III extracellular phospholipases A<sub>2</sub>: selective inhibition of group II enzymes by indomethacin but not other NSAIDs. *Agents Actions* **41**, 111–113 (1994).
65. Singh, R. K. *et al.* Aspirin induces its anti-inflammatory effects through its specific binding to phospholipase A<sub>2</sub>: crystal structure of the complex formed between phospholipase A<sub>2</sub> and aspirin at 1.9 angstroms resolution. *J Drug Target* **13**, 113–119 (2005).
66. Dennis, E. A., Cao, J., Hsu, Y. H., Magriotti, V. & Kokotos, G. Phospholipase A<sub>2</sub> enzymes: physical structure, biological function, disease implication, chemical inhibition, and therapeutic intervention. *Chem Rev* **111**, 6130–6185 (2011).
67. Zhou, X. *et al.* Structural characterization of myotoxic ecarpholin S from *Echis carinatus* venom. *Biophys J* **95**, 3366–3380 (2008).
68. Fernandes, C. A. *et al.* Comparison between apo and complexed structures of bothropstoxin-I reveals the role of Lys122 and Ca<sup>2+</sup>-binding loop region for the catalytically inactive Lys49-PLA<sub>2</sub>s. *J Struct Biol* **171**, 31–43 (2010).
69. Murakami, M. T. *et al.* Insights into metal ion binding in phospholipases A<sub>2</sub>: ultra high-resolution crystal structures of an acidic phospholipase A<sub>2</sub> in the Ca<sup>2+</sup> free and bound states. *Biochimie* **88**, 543–549 (2006).
70. Bulbring, E. Observations on the isolated phrenic nerve diaphragm preparation of the rat. 1946. *Br J Pharmacol* **120**, 3–26; discussion 21–22 (1997).
71. Soares, A. M. *et al.* A rapid procedure for the isolation of the Lys-49 myotoxin II from *Bothrops moojeni* (caissaca) venom: biochemical characterization, crystallization, myotoxic and edematogenic activity. *Toxicon* **36**, 503–514 (1998).
72. Ducruix, A. G., R. *Crystallization of Nucleic Acids and Proteins: A Practical Approach*. (Oxford University Press 1992).
73. Otwinowski, Z. & Minor, W. Processing of X-ray diffraction data collected in oscillation mode. *Macromolecular Crystallography, Pt A* **276**, 307–326 (1997).
74. Vonrhein, C. *et al.* Data processing and analysis with the autoPROC toolbox. *Acta Crystallogr D Biol Crystallogr* **67**, 293–302 (2011).
75. McCoy, A. J. *et al.* Phaser crystallographic software. *J Appl Crystallogr* **40**, 658–674 (2007).
76. Adams, P. D. *et al.* PHENIX: a comprehensive Python-based system for macromolecular structure solution. *Acta Crystallogr D Biol Crystallogr* **66**, 213–221 (2010).
77. Emsley, P. & Cowtan, K. Coot: model-building tools for molecular graphics. *Acta Crystallogr D Biol Crystallogr* **60**, 2126–2132 (2004).
78. Chen, V. B. *et al.* MolProbity: all-atom structure validation for macromolecular crystallography. *Acta Crystallogr D Biol Crystallogr* **66**, 12–21 (2010).
79. Schrodinger, LLC. *The PyMOL Molecular Graphics System, Version 1.3r1* (2010).
80. Wallace, A. C., Laskowski, R. A. & Thornton, J. M. LIGPLOT: a program to generate schematic diagrams of protein-ligand interactions. *Protein Eng* **8**, 127–134 (1995).
81. Abraham, M. J. *et al.* GROMACS: High performance molecular simulations through multi-level parallelism from laptops to supercomputers. *SoftwareX* **1–2**, 19–25 (2015).
82. Schmid, N. *et al.* Definition and testing of the GROMOS force-field versions 54A7 and 54B7. *Eur Biophys J* **40**, 843–856 (2011).
83. Olsson, M. H., Sondergaard, C. R., Rostkowski, M. & Jensen, J. H. PROPKA3: Consistent Treatment of Internal and Surface Residues in Empirical pKa Predictions. *Journal of Chemical Theory and Computation* **7**, 525–537 (2011).

84. Bussi, G., Donadio, D. & Parrinello, M. Canonical sampling through velocity rescaling. *Journal of Chemical Physics* **126**, 014101 (2007).
85. Berendsen, H. J. C., Postma, J. P. M., Vangunsteren, W. F., Dinola, A. & Haak, J. R. Molecular-Dynamics with Coupling to an External Bath. *Journal of Chemical Physics* **81**, 3684–3690 (1984).
86. Nosé, S. A molecular dynamics method for simulations in the canonical ensemble. *Molecular Physics* **52**, 255–268 (1983).
87. Hoover, W. G. Canonical dynamics: Equilibrium phase-space distributions. *Phys Rev A Gen Phys* **31**, 1695–1697 (1985).
88. Parrinello, M. & Rahman, A. Polymorphic transitions in single crystals: A new molecular dynamics method. *Journal of Applied Physics* **52** (1981).
89. Koziara, K. B., Stroet, M., Malde, A. K. & Mark, A. E. Testing and validation of the Automated Topology Builder (ATB) version 2.0: prediction of hydration free enthalpies. *J Comput Aided Mol Des* **28**, 221–233 (2014).

### Acknowledgements

Funding was provided by the Fundação de Amparo à Pesquisa do Estado de São Paulo (FAPESP), Conselho Nacional de Desenvolvimento Científico e Tecnológico (CNPq) and Coordenação de Aperfeiçoamento de Pessoal de Nível Superior (CAPES).

### Author Contributions

G.H.M.S. performed crystallographic and structural comparative analyses under supervision of M.R.M.F. A.A.S.G. performed molecular dynamics simulations under supervision of M.R.M.F. F.F.C. performed functional assays under supervision of W.L.G.C. and M.G. M.R.M.F., G.H.M.S. and F.F.C. designed, analysed the experiments and wrote the manuscript with inputs of other authors.

### Additional Information

**Competing Interests:** The authors declare no competing interests.

**Publisher's note:** Springer Nature remains neutral with regard to jurisdictional claims in published maps and institutional affiliations.



**Open Access** This article is licensed under a Creative Commons Attribution 4.0 International License, which permits use, sharing, adaptation, distribution and reproduction in any medium or format, as long as you give appropriate credit to the original author(s) and the source, provide a link to the Creative Commons license, and indicate if changes were made. The images or other third party material in this article are included in the article's Creative Commons license, unless indicated otherwise in a credit line to the material. If material is not included in the article's Creative Commons license and your intended use is not permitted by statutory regulation or exceeds the permitted use, you will need to obtain permission directly from the copyright holder. To view a copy of this license, visit <http://creativecommons.org/licenses/by/4.0/>.

© The Author(s) 2019